# DETECTION OF MECHANICAL STRESS LIMITING EFFECTS OF CRANE STRUCTURE DEFORMATION

**LEOPOLD HRABOVSKY [1], ZDENEK FOLTA [2]**

[1] Institute of Transport
[2] Department of Machine Parts and Mechanisms
VSB-Technical University of Ostrava, Faculty of Mechanical Engineering, Ostrava-Poruba, Czech Republic

The paper presents a construction design and results of laboratory tests of so-called mechanical stress detectors, which can be used to detect the deformation of the steel structure of a crane and to amplify the mechanical signal from the effect of the so-called crane skewing, which is included among occasional loads acting on the crane. The values of the relative elongation of the detectors corresponding to the magnitude of the instantaneous tensile force were obtained by conducting experimental mechanical tests. Detectors of a known extent of deformation were installed on a two-girder overhead crane bridge, where they measured axial forces generated during the controlled deformation of the crane bridge. In practice, the instantaneous values of the axial forces recorded by the individual detectors make it possible to regulate the speed of the crane drive wheels and thus eliminate, in a relatively short time, the undesirable effects of deforming the crane bridge and friction of the crane wheels on the sides of the rail heads.

**KEYWORDS**

mechanical stress detector, double girder overhead crane, deformation of steel structure, crane skewing.

## 1 INTRODUCTION

Malingment or jamming of cranes [730035 1998], [270103 1991], [270110 1993], [270105 2015] resulting from the degradation of steel structures of cranes associated with what is referred to in professional literature as "crane skewing", of an overhead-type crane, is the accompanying phenomenon of work modes based on geometry and the principle of their functioning. The random process of crane jamming goes hand in hand with the deformation of load bearing steel constructions on a horizontal plane on the crane runway.

During the travel of cranes on a fixed track, formed by crane rails, undesired skewing occurs [Hannnover 1970], [Forestier 1973]. Skewing causes additional loads [Hrabovsky 2016], [Musilek1 2019], [Sostakov 2014], especially in the horizontal direction, which adversely affects the crane track (formed by rails), travel wheels [Bosso 2016], [Braghin 2006], but also on the crane construction itself [Lobov1 1982].

Additional loads of a similar nature can be observed when braking the crane [Hrabovsky 2016], with the effect of additional loads, i.e., the horizontal forces between the crane and the crane track. Due to the asymmetry of the positioning of the trolley (the block moves along the length of the crane bridge) and the load suspended on it, the more loaded side of the crane "overtakes" the crossbeam fitted with the travel drive unit compared to the other side. Overtaking of the more loaded side of the crane compared to the other, less loaded, side causes an additional load on the crane's main girder similar to the effects of the load caused by skewing, but quite often with significantly greater effects.

A comparison of computational models of forces from the skewing of a crane on a crane track was performed in [Musilek1 2019] by Musílek. The paper [Sostakov 2014], provides an algorithm, supplementary comments and numerical examples that point out the main phases of skewing forces, according to the standard EN 15 011.

There are a number of procedures for determining the horizontal forces from the skewing of the bridge crane's crossbeam, some of which are listed in the valid Czech standards [730035 1998], [270103 1991], [270110 1993], [270105 2015].

In [Musilek2 2019] states that the most significant load caused by motion of crane is the skewing. In the past, the cause of the skewing was considered to be caused by different speeds of the end-carriages of the crane which result to the horizontal transverse loads of the crane runway. In the present, the skewing of crane is defined as the motion of the overhead bridge crane with the constant velocity, but with the angle relative to the crane runway.

Kuľka et al. describe in [Kulka 2020] the placement of strain gauges sensing the deformation on both crossbeams at places close to the connection of the crossbeams to the main beams.

Zelić et al. [Zelic 2018] presents an experimental determination of lateral forces acting on the vertical wheels of a bridge crane using two different solutions of transducers for the direct measurement on the wheels of the cranes in operation, without changing the way of lateral guiding.

Jendel and Berg [Jendel 2003] simulated and measured wheel profiles during operational wear and achieved satisfactory results.
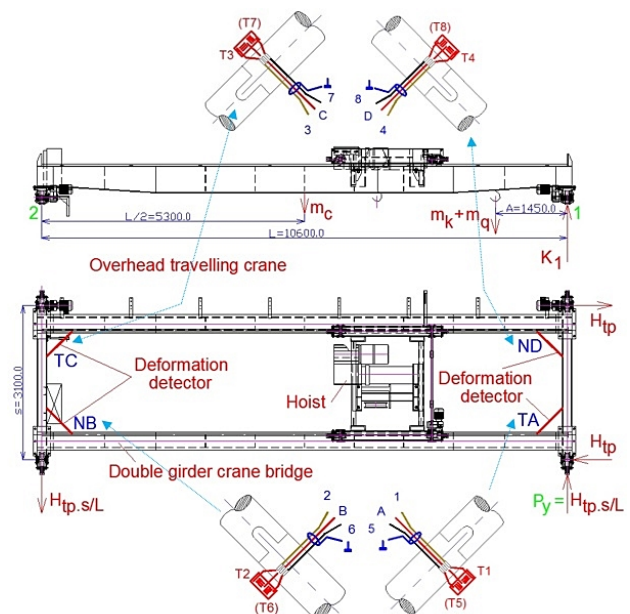


**Figure 1.** Double girder overhead crane - 15T-10.6x3.1

Ramalho et al. [Ramalho 2013] investigated the effect of contact conditions on friction and wear behavior of carbon and low alloy wheel/rail steel.

Lobov [Lobov2 1984], [Lobov3 1986], [Lobov4 1989] created dynamical model describing motion of the overhead bridge crane. This model enables to determinate the horizontal transverse forces. The model considers the crane as the rigid body with the load of crab rigidly connected to the crane. It

means that the swinging of the load on the crab rope was neglected.

Mitrovic et al. [Mitrovic 2009] describes an algorithm which provides load sharing proportional to the rated motor power on the simple and practically applicable method on the basis of estimated torques by frequency converters, and controller realized in PLC.

## 2 CRANE STRUCTURE, SKEW FORCE

To verify whether the actual effects of mechanical tension (Figure 3) from the deformed steel structure of the overhead crane are suitably amplified by mechanical stress detectors (Figure 5), an overhead double girder crane indicated as 15T-10.6x3.1, with a load capacity of 15 tons, was used. The basic geometric dimensions of the crane; including showing the location of the mechanical stress detectors at the corners (i.e. the points of connection of the main girders to the crossbeams) of the crane bridge, are shown in Figure 1. The basic parameters of the crane are given in Table 1. The basic dimensions and static values of the cross section of the crossbeam and the main girder of the closed, box cross-section design are shown in Figure 2.
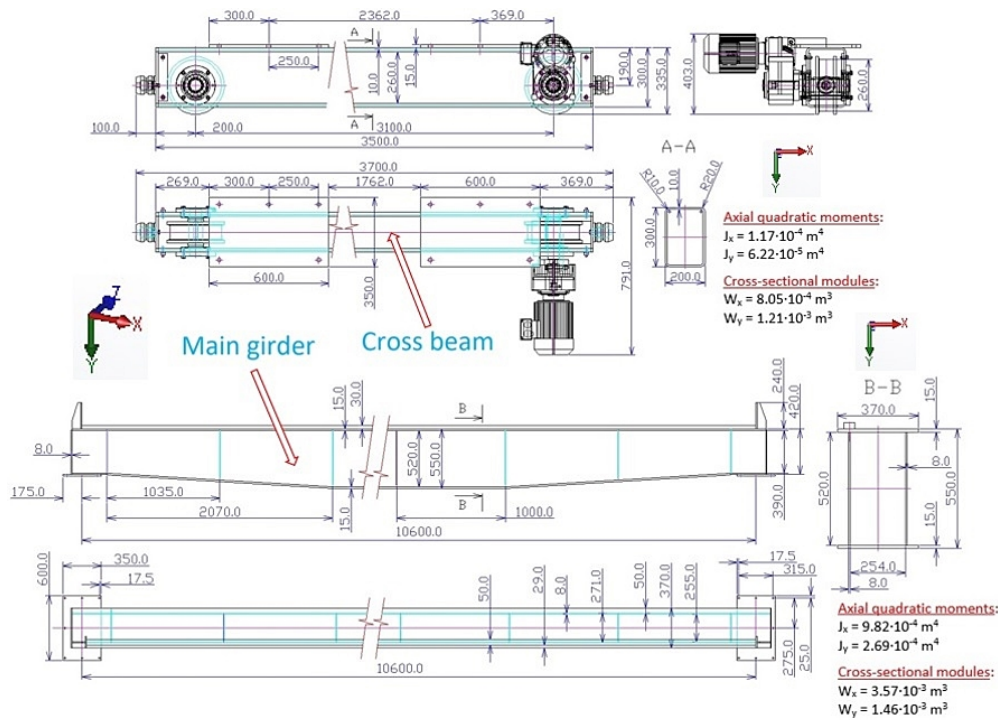


**Figure 2.** Double girder overhead crane, 1) cross beam, 2) main girder of the closed box cross-section design

It is possible to determine the value of the horizontal lateral force from the skew of the crane on the crane track $H_{tP}$ (3) and the value of the force acting in the direction of travel of the crane $P_y$ (5) using the calculation methodology given in [270103 1991], [Transducer 2010].

| Rated load $m_q$ [kg] | 15000 |
|---|---|
| Total weight of crane $m_c$ [kg] | 6892.3 |
| Weight of load block $m_k$ [kg] | 1945.6 |
| Runway length $L$ [mm] | 10600 |
| Wheelbase $w$ [mm] | 3100 |
| Block travel limit $L_1$ [mm] | 1450 |

**Table 1.** Basic parameters of double girder overhead crane

$$\lambda = 0.025 \cdot \frac{L}{s} = 0.025 \cdot \frac{10.6}{3.1} = 0.085 \qquad (1)$$

$$K_1 = \frac{(m_c - m_k) \cdot g \cdot \frac{L}{2} + (m_k + m_q) \cdot g \cdot (L - L_1)}{L} = 167.7 \cdot 10^3 \ N \qquad (2)$$

where $K_1$ is the load on the wheels or rocker arms of the crane undercarriage on the more loaded branch of the crane track

from the net weight of the crane and the cat with the total load in the most efficient position.

$$H_{tP} = \lambda \cdot K_1 = 0.085 \cdot 167.7 \cdot 10^3 = 14.34 \cdot 10^3 \ N \qquad (3)$$

$$H_{tP} \cdot \frac{s}{L} = 14.34 \cdot 10^3 \cdot \frac{3.1}{10.6} = 4.19 \cdot 10^3 N \qquad (4)$$

$$P_y = H_{tP} \cdot \frac{s}{L} \cdot \gamma_{tP} = 4.19 \cdot 10^3 \cdot 1.1 = 4.61 \cdot 10^3 \ N \qquad (5)$$

The calculated value of the deformation force acting in the direction of travel of the crane is determined by rounding $P_y = 5 \cdot 10^3 \ N$.

## 3 DEFORMATION OF THE STEEL STRUCTURE OF THE CRANE, MEASURING ELEMENT LOAD

From the shape and type of the steel structure of the crane it is possible to analyse several deformation shapes - for example [Hrabovsky2 2021], see Figure 3 - which lead to symmetrical or asymmetrical deformations of the frame supporting structure of the crane, resp. to combinations of these shapes of deformations on individual elements of the steel structure of the crane. Precise skew analysis is, among other things, associated with online monitoring of the horizontal plane of the

crane.

To obtain the values of tensile/compressive forces acting on component detectors of mechanical stresses (TA, NB, TC and ND, see Figure 1) located at the points where the main girders (Figure 2a) mechanically connect to the crossbeams (Figure 2b) of the double girder overhead crane, a 3D model of the steel structure of the crane bridge was created - see Figure 3. The steel structure of the crane was loaded with a horizontal force $P_y$ in the travel direction of the crane bridge and, by means of the finite element method, the axial forces acting in the places of installed mechanical stress detectors were determined. Due to the load on the released right side of the travel by the force $P_y$, there is a horizontal displacement of the right cross beam relative to the braked, opposite left side of the crane of $D_y = 6.84$ mm - see Figure 3.

The maximum axial force, calculated by the finite element method, at the point of the installed mechanical amplifier is $F_{45} = -17.2 \cdot 10^3$ N.
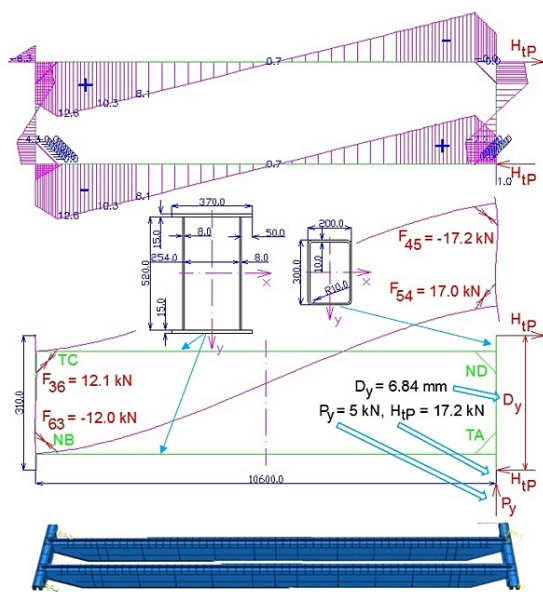


**Figure 3.** Deformation of steel structure of crane bridge

### 3.1 Measuring system, location and specification of the strain gauge

Measurement and evaluation chain diagram is illustrated in Figure 4.

There were chosen the strain gauges 1-LY11-6/350 [Gauges 2006] produced by the company HBM. The ohmic resistance value of the applied sensors was 350 Ω. The gluing process was performed using the two-part glue X 60, which is specified for the strain gauge applications.

The strain gauges, installed on the measuring part (2, Figure 5) were insulated against external influences by means of a silicon rubber SG 250. Transmission of signals from the sensors into the measuring apparatus was realized by means of shielded input cables. The applied measuring apparatus was an oscilloscope and portable data acquisition recorder Yokogawa.
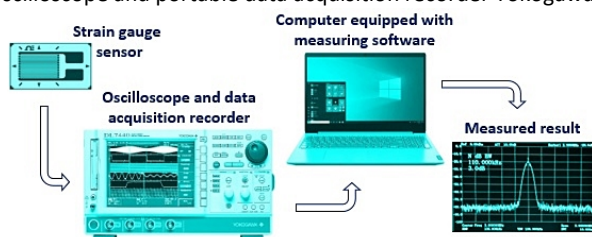


**Figure 4.** Measuring amplifier and measurement chain diagram

### 3.2 Structural and strength design of measuring components

Material 11523.1, from which the measuring component (2, Figure 5) of the ϕ 30/25 mm mechanical stress detector is made, acquires a yield strength $R_e = 275 \cdot 10^6$ Pa. If we assume that the measuring components (taped over with foil strain gauges 1-LY11-6/35) will be loaded to a maximum of 30% of the yield strength $R_e$ ($R_{ev} = 0.3 \cdot R_e = 82.5 \cdot 10^6$ Pa) then, at the maximum axial force $P_y$, an axial force of maximum magnitude $F = 17.2 \cdot 10^3$ N (see Figure 3) acts at the component measuring points of the mechanical stress detector. The minimum cross-section $S_{min}$ of the measuring component of the mechanical stress detector can be determined according to (6).

$$\sigma = \frac{F}{S_{min}} \Rightarrow S_{min} = \frac{F}{R_{ev}} = \frac{17.2 \cdot 10^3}{82.5 \cdot 10^6} = 2.08 \cdot 10^{-4} \ m^2 \qquad (6)$$

Measuring component of the mechanical stress detector, see Figure 5, with its actual cross section $S_s$ (7) is designed as a tube with an outer diameter $D = 30$ mm and an inner diameter $d = 25$ mm.

$$S_S = \frac{\pi \cdot \left(D^2 - d^2\right)}{4} = \frac{\pi \cdot \left(0.03^2 - 0.025^2\right)}{4} = 2.16 \cdot 10^{-4} \ m^2 \qquad (7)$$

The maximum applied stress $\sigma_m$ in the measuring component 2 of the mechanical stress detector is expressed in relationship (8).

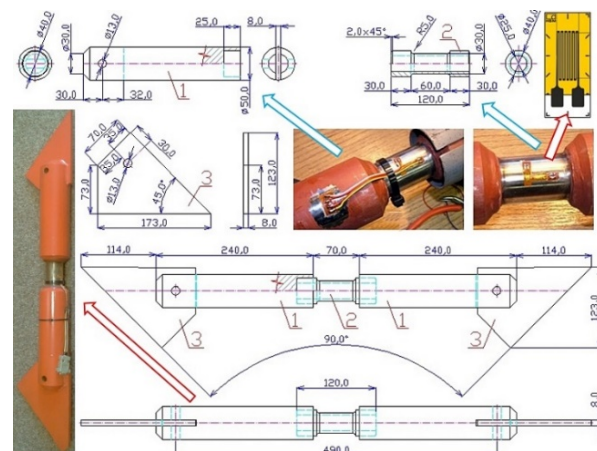$$\sigma_m = \frac{F}{S_S} = \frac{17.2 \cdot 10^3}{2.16 \cdot 10^{-4}} = 79.64 \cdot 10^6 \ Pa \qquad (8)$$



**Figure 5.** Dimensional parameters of mechanical stress detector components

### 3.3 Testing equipment for mechanical stress detectors

Verification of the correctness of the functional properties of the construction designed mechanical stress detectors (Figure 5) was performed in the Laboratory of Research and Testing at the Institute of Transport, Faculty of Mechanical Engineering of VSB - Technical University of Ostrava, on the constructed testing device Figure 6.

The testing device consists of two main parts 1 and 2, slidable against each other in the vertical direction, see Figure 6. The tensile force in the mechanical stress detector is exerted by a hydraulic jack 4 with a load capacity of $3 \cdot 10^3$ kg. The instantaneous value of the tensile force $F$ is detected by the tensile force sensor C2-5T 3 [Transducer 2010]. A plate (7, Figure 7) is welded to the lower surface of the beam of the stationary part 1 of the testing device. A hub 8 is fastened to

the plate 7 by screws, into the opening of which the cylindrical part of the sensor 3 is guided.

When the hydraulic jack 4 is activated, the moving part 2 of the test device is pushed away from the stationary part 1. The magnitude of the pushing force $F_m$ (see Table 2) exerted by the hydraulic jack 4 is detected by the sensor 3. The tensile force acting on the detector is detected by foil resistance strain gauges on part 2 (see Figure 5) and recorded with a Yokogawa DL750 digital oscilloscope.
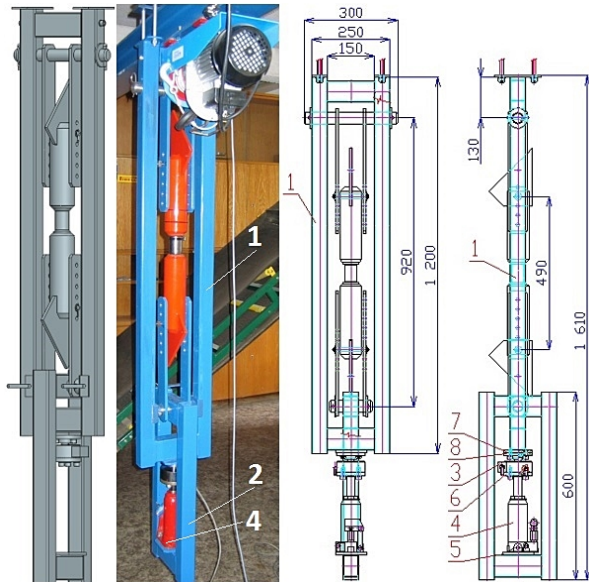


**Figure 6.** Testing device for mechanical stress detectors

## 4 MEASURING, MEASUREMENT DATA

### 4.1 Experimental tests of mechanical stress detectors

For the calibration of mechanical stress detectors, the Yokogawa DL750 measuring apparatus was used, in which relation (10) is used to calculate the sensed value of stress $\sigma_m$ of the deformed cross section of a test rod glued with resistance foil strain gauges [Folta 2015, pp.13]. According to relationship (9), it is possible to determine the output voltage from the strain gauge bridge $U_c$ to the tensile force sensor (3, Figure 5 and Figure 7) when deriving the tensile force $F$ by a hydraulic jack (4, Figure 6).
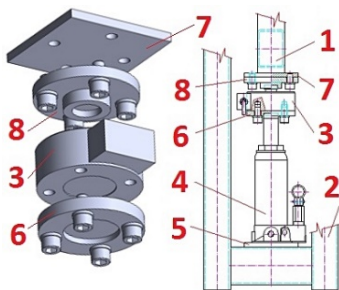


**Figure 7.** Derivation of pressure force by hydraulic jack and detection of its magnitude by sensor

Assuming that at the maximum possible load of the tensile force sensor, $5 \cdot 10^3\ kg \cong 50\ kN$, it is possible to read the value of voltage $U = 1\ V$ at 1000 times gain at the supply voltage $U_N = 5\ V$ of the pressure force sensor C2-5T, then the voltage $U_c = 0.88\ mV/V$ corresponds to tensile force $F = 22.00\ kN$ (9), see Table 2.

$$\frac{2\ mV/V\ ...\ 50\ kN}{U_C\ [mV/V]\ ...\ 22\ kN} \Rightarrow U_c = \frac{22 \cdot 50}{2} = 0.88\ mV/V \tag{9}$$

For verifying the functional properties of the mechanical stress detector (Figure 5) on the testing equipment (Figure 6), the mechanical stress detectors were subjected to a tensile force $F$ exerted by the compressive force of the hydraulic jack 4, the instantaneous value of which was detected by the tensile force sensor 3. The instantaneous stress value $U_c$ for the exerted tensile force $F$ is read on the display of the Yokogawa DL750 measuring apparatus, and the display also shows a graphical waveform of the stress value $U_m$, see Table 2.

| Detector | C2-5T detector | | Measuring component of detector | | |
|---|---|---|---|---|---|
| | $U_c$ [mV/V] | $F$ [kN] | $U_m$ [mV/V] | $k_m$ [kN/mV/V] | $\sigma_m$ [MPa] |
| **TA** | 0.880 (9) | 22.00[*1] | 0.381[*1] | 57.74 | 59.75 (10) |
| **NB** | 0.896 | 22.40[*2] | 0.370[*2] | 60.54 | 58.11 |
| **TC** | 0.860 | 21.50[*3] | 0.293[*3] | 73.38 | 45.95 |
| **ND** | 0.845 | 21.13[*4] | 0.330[*4] | 64.03 | 51.76 |

[*1] see Figure 8, [*2] see Figure 9, [*3] see Figure 10, [*4] see Figure 11

**Table 2.** Material properties of SCP10

$$\sigma_m = \frac{4 \cdot U_m \cdot E}{k \cdot n_t \cdot 10^3} = \frac{4 \cdot 0.381 \cdot 2.1 \cdot 10^{11}}{2.06 \cdot 2.6 \cdot 10^3} = 59.75\ MPa \tag{10}$$

where $n_t = 2.6$ for the total number of strain gauges used 4 (of which 2 strain gauges are glued longitudinally and measure longitudinal elongation and 2 strain gauges are glued transversely and measure transverse contraction. $n_t = 2 + 2 \cdot \mu = 2.6$, pro $\mu = 0.3$).

Each mechanical stress detector (TA, NB, TC and ND, see Figure 1 and Figure 2) was repeatedly subjected to a tensile force $F$ of known magnitude induced by the compressive force of the hydraulic jack 5 times under identical input conditions. Figures 8-11 show a record of one experimental test of each of the four monitored mechanical stress detectors (Figure 4), out of the whole range of experimental records obtained.

### 4.2 Deformation detection of the stell structure of the crane

After welding the detectors to the inner corners of the 15T-10.6x3.1 crane bridge (Figure 13), the crane trolley was placed in the middle of the span of the two-girder overhead crane bridge.
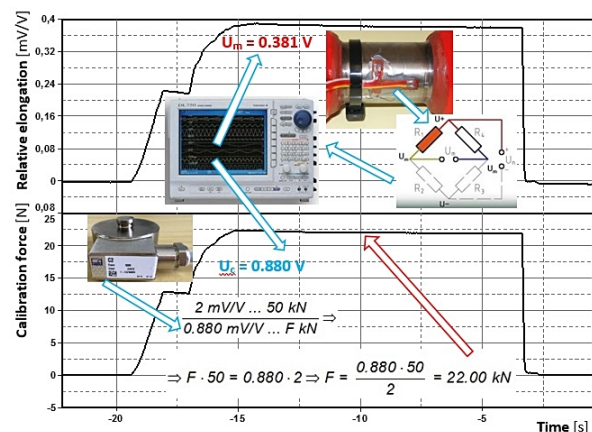


**Figure 8.** Record of the experimental test of the TA detector

In the described crane, the skew phenomenon of a bridge crane was simulated by a horizontal displacement of the right crossbeam of the crane in the direction of travel of the crane under the condition where the travel wheel of the opposite crossbeam on the crane rail was fixed against forward displacement. The compressive force $P_y$ (5) was exerted in the direction of travel of the crane bridge on the front surface of the crossbeam (Figure 2) by a hydraulic jack 4, which was placed on the designed platform P (Figure 12).
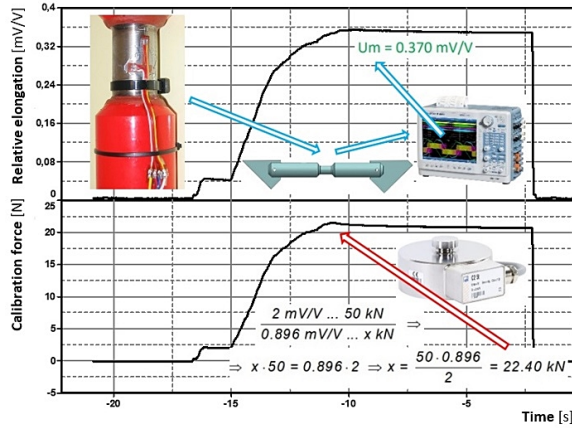


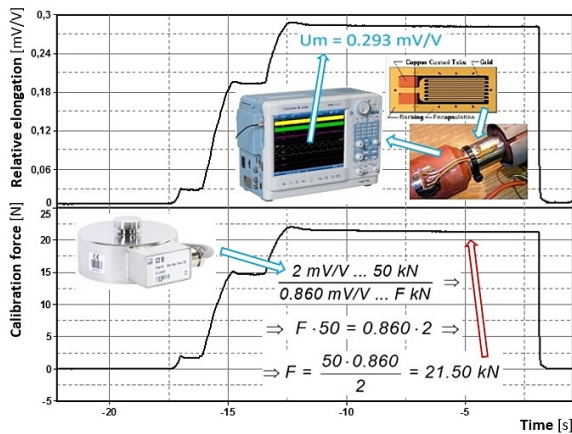**Figure 9.** Record of the experimental test of the NB detector



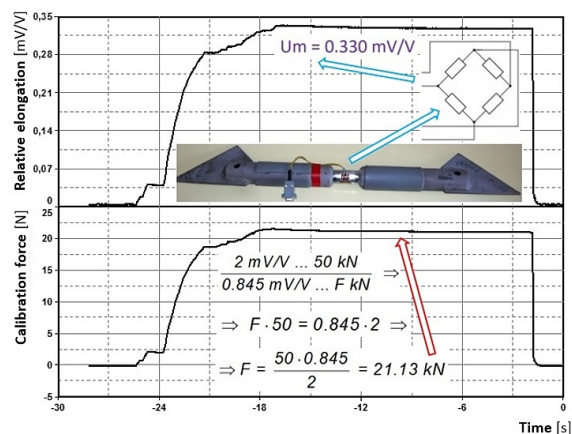**Figure 10.** Record of the experimental test of the TC detector



**Figure 11.** Record of the experimental test of the ND detector

During the experimental tests, the purpose of which was to detect the deformation of the steel structure of the crane, the platform was mechanically attached to the beam of the steel structure at the end of the crane track.

Figure 13 presents in its lower part the time course of the hydraulic jack 4, see Figure 12, the forces $P_y$ generated into the crossbar, which were detected by the sensor 4. In the upper part of Figure 13 shows the waveforms of instantaneous values of the acting axial forces of individual detectors TA, NB, TC and ND.

### 4.3 Axial forces derived from the effects of crane bridge deformation

After removing the special rail stop (its construction is not specified) and releasing the fixed castor wheel (see chapter 4.2) and removing the parts assembly, which exerted and detected the compressive force $P_y$, the detector connectors were connected by shielded cables to the Yokogawa measuring apparatus.
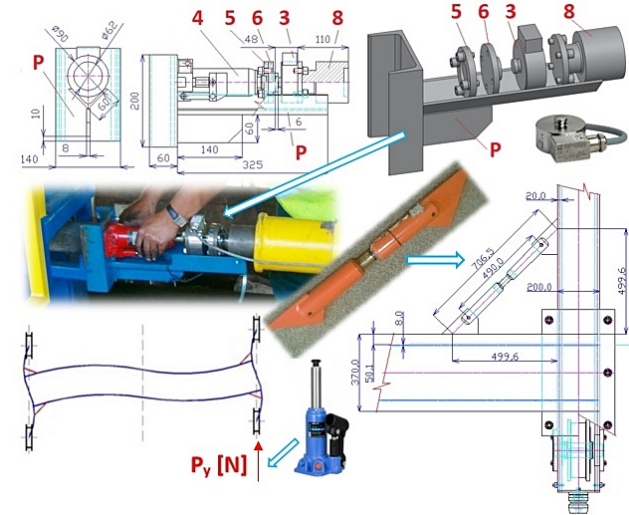


**Figure 12.** Platform P supporting the set of components exerting and detecting compressive force $P_y$

The crane was repeatedly driven in both directions of the crane track under the condition where the crane trolley, unloaded, was in the middle of the span of the bridge of the two-girder overhead crane. The crane was then moved to the end of the crane track, and it was checked, on all four wheels, that the distance between the two wheels on the sides of the rail head was the same.
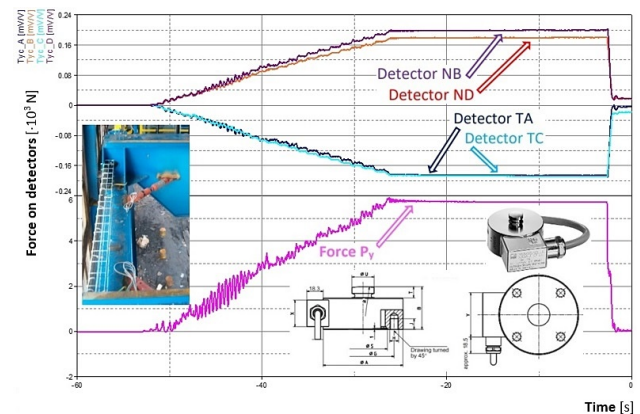


**Figure 13.** Axial forces detected by detectors from the deformation of the crane bridge induced by the deformation force $P_y$ into the crossbeam, acting in the direction of travel of the crane

The crane, in different conditions simulating the actual operating conditions (for example, with the trolley loaded with the maximum rated load, or without a load, was in the extreme position, or in the middle, of the span of the bridge; start/braking of the crane with a connected/disconnected load, etc.) was driven along the crane track and the values of the axial forces generated to component detectors were recorded, see Figure 14.

## 5 CONCLUSION

To detect additional loads acting on the steel structure of the crane from skewed operation, 4 units of structurally identical mechanical stress detectors were used - see Figure 5. The key parts of the detectors are the measuring components (2, Figure 5), which were, for the purposes of detecting additional loads from skewing of the crane, carefully machined and were completely identical for all detectors.
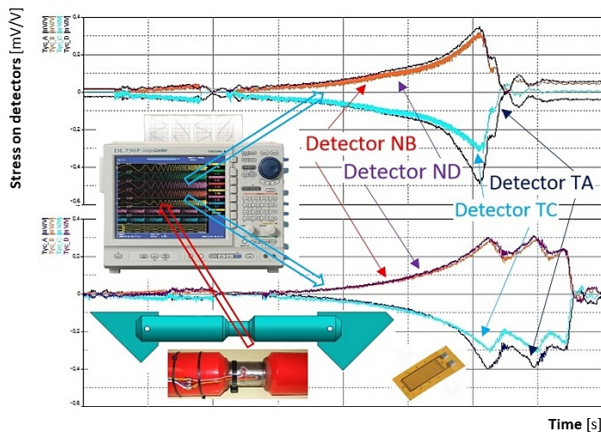


**Figure 14.** Axial forces detected by detectors from the deformation of the bridge during crane travel

The application point and the place where the foil resistance strain gauges were glued to the measuring component of the individual detectors, were carefully determined and were completely identical for all mechanical stress detectors. A measuring element with a total length of *120 mm*, see Figure 5, is comprised of two end portions of an outer diameter of *40 mm*, each *30 mm* long and a central portion having an outer diameter of *30 mm* and a length of *60 mm*. Two foil resistance strain gauges (one longitudinally and the other transversely) were glued to the central part of the measuring component of each of the detectors. The results of testing and calibration of mechanical voltage detectors show that, even when maintaining strictly identical input, and also test conditions, the individual members of the detectors give a different value of relative elongation $\varepsilon$ [-]. The highest value of relative elongation was recorded for the TA detector, see Table 2, and the lowest for the TC detector. The difference in the relative elongation of the individual measuring components (completely identical dimensions) can be justified by the non-compliance with the practical requirement for the length of the rod $L_r$ [m], which should be at least three times the diameter of the rod $D_r$ [m]. The selected length/diameter ratio of the measuring component $60/30 = 2$ leads, during its axial loading by tensile/compressive force, to an undesirable redistribution of stress and direction of intersecting lines of force along the cross-section, with the result that the value of actual relative elongation does not coincide with theoretical value. By installing detectors in the inner corner spaces of the double-girder crane bridge according to Figure 1, after deriving a horizontal displacement in the direction of travel of the crane of the right crossbeam (assuming fixation of the left cross member), axial forces were detected, see Figure 13. The instantaneous values and waveforms recorded by the axial force detectors correspond to the theoretical assumption of the deformation of the steel structure of the double-girder crane bridge from the random effect of the skew (skewed operation). From the results of obtained graphs of recorded wave⍰forms of axial forces by mechanical stress detectors during experimental tests performed in laboratory conditions, but especially from recording of detected forces detectors in operating conditions, it can be concluded that it is advantageous to use mechanical stress detectors to sense deformation of steel structure of overhead type cranes. Through precise analysis, which results in accurate knowledge of the deformation, stress and deformation of the crane frame structure, it is possible to structurally design mechanical stress detectors to amplify the effects of mechanical stress in the sections of the steel structure of the crane where the installation of detectors is under consideration, using the numerical FEM method. Component strain gauges of individual detectors installed in the inner corners of the crane bridge can be conveniently connected to the Wheatson bridge and the resulting electrical signal output can be used to control the frequency converters of the crane travel units as specified in PUV1997-7213 entitled "Device for restricting misalignment between wheel and track of rail vehicles, particularly cranes".

## REFERENCES

**[Bosso 2016]** Bosso, N., Soma, A. and Zampieri, N. Bridge cranes wheels and rails: Wear analysis. Civil-Comp. Proc, 2016, Vol. 110, pp. 1-14.

**[Braghin 2006]** Braghin, F., Lewis, R., Dwyer-Joyce R.S. and Bruni, S. A mathematical model to predict railway wheel profile evolution due to wear. Wear, 2006, Vol. 261, pp. 1253-1264.

**[Braghin 2006]** Braghin, F., Lewis, R., Dwyer-Joyce R.S. and Bruni, S. A mathematical model to predict railway wheel profile evolution due to wear. Wear, 2006, Vol. 261, pp. 1253-1264.

**[Forestier 1973]** Forestier, R. Comments on the calculation of the horizontal forces due to the rolling ones. Metallic Constructions, 1973, vol. 1.

**[Folta 2015]** Folta, Z. Odporova tenzometrie, 2015 [3.8.2021] Available at: https://slideplayer.cz/slide/12090281

**[Hannover 1970]** Hannover, H. O. Horizontal forces and inclination course on a bridge crane in the Beharungsfahrt. Steel and Iron, 1970, vol. 26.

**[Hrabovsky1 2016]** Hrabovsky, L. Action on crane runway caused by horizontal forces due to crane skewing. Key Engineering Materials, October 2016, vol. 669, pp. 391-399.

**[Hrabovsky2 2021]** Hrabovsky, L., Cepica, D. and Frydrysek, K. Detection of Mechanical Stress in the Steel Structure of a Bridge Crane. Theoretical and Applied Mechanics Letters, 2021, Vol. 11, No. 5, p. 100299.

**[Kulka 2020]** Kulka, J., Mantic, M., Fedorko, G. and Molnar, V. Failure analysis concerning causes of wear for bridge crane rails and wheels. Engineering Failure Analysis, Maech 2020, vol. 110, p. 104441.

**[Lobov1 1982]** Lobov, N. A. Loads of an overhead travelling crane caused by transverse and rotatory motions of the bridge girder. Bulletin of Machine Building, 1982, Vol. 62.

**[Lobov2 1984]** Lobov, N. A. Loads of an overhead travelling crane caused by transverse and rotatory motions of the bridge girder. Vestnik Mashinostroeniya, 1984, Vol. 64, pp 22-26.

**[Lobov3 1986]** Lobov, N. A. Loads on an overhead travelling crane when it moves with a constant skew setting of the girder. Vestnik Mashinostroeniya, 1986, Vol. 66, pp. 13-17.

**[Lobov4 1989]** Lobov, N. A., Masyagin, A. V. and Dulev, A. V. On lengthening the life of bridge crane track wheels. Vestnik Mashinostroeniya, 1989, Vol. 69, pp. 30-34.

**[Musilek1 2019]** Musilek, J. Horizontal forces on crane runway caused by skewing of the crane. IOP Conference Series: Materials Science and Engineering, 2019, Vol. 471, No. 5, p. 052001.

**[Musilek2 2019]** Musilek, J. Dynamical Model for Determination of Horizontal Forces on Crane Runway during Motion of the Crane. IOP Conference Series: Materials Science and Engineering, 2019, Vol. 603, No. 5, p. 052076.

**[Mitrovic 2009]** Mitrovic, N. Kostic, V. Petronijevic M. and Jeftenic, B. Multi-motor drives for crane application. Advances in Electrical and Computer Engineering, 2009, Vol. 9, No.3, pp.57-62.

**[Jendel 2003]** Jendel, T. and Berg, M. Prediction of wheel profile wear: Methodology and verification, Veh. Syst. Dyn, 2003, Vol. 37, pp.502-513.

**[Ramalho 2013]** Ramalho, A., Esteves M. and Marta, P. Friction and wear behaviour of rolling-sliding steel contacts. Wear, 2013, Vol. 302, No. 1-2, pp. 1468-1480.

**[Sostakov 2014]** Sostakov, R., Zelic, A., Knezevic, I., Zuber N. and Rafa, K. Application of rigid method for determining the skewing forces on bridge cranes and trolleys according to EN 15 011. Machine design, 2014, Vol. 6, No. 2.

**[Zelic 2018]** Zelic, A., Zuber, N. and Sostakov, R. Experimental determination of lateral forces caused by bridge crane skewing during travelling. Eksploatacja i Niezawodnosc, 2018, Vol. 20

**[730035 1998]** ENV 1991-5:1998 Eurocode 1: Basis of design and actions on structures - Part 5: Actions induced by cranes and other machinery (In Czech : CSN P ENV 1991-5 (730035): Zasady navrhovani a zatizeni konstrukci - Cast 5: Zatizeni od jerabu a strojniho vybaveni. 1998).

**[270103 1991]** CSN 27 0103 Design of steel crane structures. Calculation according to the limit state methods (In Czech : CSN 27 0103 (270103): Navrhovani ocelovych konstrukci jerabu. Vypocet podle meznich stavu. 1991.)

**[270103 1991]** CSN 27 0103 Design of steel crane structures. Calculation according to the limit state methods (In Czech : CSN 27 0103 (270103): Navrhovani ocelovych konstrukci jerabu. Vypocet podle meznich stavu. 1991.)

**[270110 1993]** ISO 8686-1:1989 Cranes: Design principles for loads and load combinations. Part 1: General. (In Czech : CSN ISO 8686-1 (270110): Jeraby. Zasady vypoctu zatizeni a kombinaci zatizeni. Cast 1: Vseobecne. 1993.)

**[270105 2015]** EN 13001- 2:2002 Crane safety - General design - Part 2: Load actions. (In Czech : CSN EN 13001-2 (270105) Jeraby - Navrh vseobecne - Cast 2: Ucinky zatizeni. 2015.)

**[Transducer 2010]** C2 Force Transducer, 2010 [21.11.2020] Available at: https://www.hbm.cz/wp-content/uploads/B00656.pdf

**[Gauges 2006]** Strain Gauges. First choice for strain measurements, 2006 [8.4.2020] Available at: www.hbm.cz/wp-content/uploads/S01265.pdf

**CONTACTS:**

doc. Ing. Leopold Hrabovsky, Ph.D.
VSB-Technical University of Ostrava,
Faculty of Mechanical Engineering,
Institute of Transport,
17. listopadu 15/2172, 708 00 Ostrava - Poruba, Czech Republic,
leopold.hrabovsky@vsb.cz

doc. Ing. Zdenek Folta, Ph.D.
VSB-Technical University of Ostrava,
Faculty of Mechanical Engineering,
Department of Machine Parts and Mechanisms,
17. listopadu 15/2172, 708 00 Ostrava - Poruba, Czech Republic,
zdenek.folta@vsb.cz